Heliyon 11 (2025) e41929

Contents lists available at ScienceDirect

Heliyon

journal homepage: www.cell.com/heliyon

Research article

Amorphous calcium phosphate-coated surfaces as a model for bone microenvironment in prostate cancer

Rebeca San Martin [a,1], Prijoyit Das [b], Tianchun Xue [b], Morgan Rose Brown [a], Renata Dos Reis Marques [a], Michael Essington [c], Adrian Gonzalez [d], Rachel Patton McCord [a,*]

[a] Department of Biochemistry & Cellular and Molecular Biology, University of Tennessee, 309 Ken and Blaire Mossman Bldg. 1311 Cumberland Ave, Knoxville, TN, 37996, USA
[b] UT-ORNL Graduate School of Genome Science and Technology, University of Tennessee, 309 Ken and Blaire Mossman Bldg. 1311 Cumberland Ave, Knoxville, TN, 37996, USA
[c] Department of Biosystems Engineering and Soil Science. University of Tennessee, Institute of Agriculture, 2621 Morgan Circle, Knoxville, TN, 37996, USA
[d] Water Quality Core Facility. Department of Civil and Environmental Engineering, Tickle College of Engineering. University of Tennessee, 325 John D. Tickle Engineering Building 851 Neyland Drive, Knoxville, TN, 37996, USA

ARTICLE INFO

Keywords:
Prostate cancer
Bone metastasis
Amorphous calcium phosphate
Cell culture modeling
Androgen resistance
Gene expression

ABSTRACT

Background: Bone metastasis remains one of the biggest challenges in the treatment of prostate cancer, and other solid tumors such as breast, lung, and colon. Modeling a complex microenvironment in-vitro such as the bone niche, requires interrogation of cell-cell interactions, specific extracellular matrix proteins, and a high calcium environment.
Methods: Here, we present a fast and cost-effective system in which commercially available, non-adhesive cell culture vessels are coated with amorphous calcium phosphate (ACP) as a surrogate for bone matrix. We also present modified protocols for subculturing cells and collecting nucleic acids and protein in high-calcium samples.
Results: We find that prostate epithelial cell lines show increased adhesion and proliferation when cultured in these amorphous calcium surfaces, accompanied by independence from androgen starvation. We observe gene expression changes on ACP surfaces in early adenocarcinoma cell lines which match alterations relevant to prostate cancer progression.
Conclusions: Incorporating biologically relevant in-vitro systems that address the microenvironment milieu of the metastatic site is essential for accurately modeling cancer progression. In the case of bone metastasis, calcium availability, uptake, and downstream signaling are of paramount importance for the survival of the cancer cell and should be considered in the development of preclinical models.

* Corresponding author.
E-mail addresses: rebeca.sanmartin@einsteinmed.edu (R. San Martin), das@molbio.mgh.harvard.edu (P. Das), txue@vols.utk.edu (T. Xue), mobr7318@colorado.edu (M.R. Brown), rdosreismarques@ucsb.edu (R. Dos Reis Marques), messington@utk.edu (M. Essington), agonza17@utk.edu (A. Gonzalez), rmccord@utk.edu (R.P. McCord).
[1] Present address: Montefiore Einstein Comprehensive Cancer Center, Cancer Dormancy Institute, Albert Einstein College of Medicine, Bronx, NY, 10461.

https://doi.org/10.1016/j.heliyon.2025.e41929
Received 1 October 2024; Received in revised form 9 January 2025; Accepted 12 January 2025
Available online 18 January 2025

List of abbreviations

ACP	amorphous calcium phosphate
RWPE	non-tumorigenic prostate epithelial cells
LNCaP	adenocarcinoma cell line
VCaP, MDAPCa2a	bone metastatic cell lines
SEM	scanning electron microscopy
XRD	X-ray diffraction
DHT	dihydrotestosterone
KSF	chemically defined media that does not contain serum
FNC	fibronectin and collagen coating
ADT	androgen deprivation therapy
Hi-C	chromosome conformation capture

1. Background

Prostate cancer remains a challenge in healthcare in the United States since it is the most commonly diagnosed malignancy in men, with about three hundred thousand new cases estimated in the United States for 2024. Of these patients, about eleven percent are expected to succumb to the disease [1], with about ninety percent of patients diagnosed with late-stage prostate cancer presenting bone metastases [2]. Importantly, patients diagnosed with localized prostate cancer can present with circulating tumor cells [3–5] that can invade other tissues and develop subclinical micro-metastases. Unfortunately, the organotropic mechanisms that mediate prostate cancer colonization to the bone are poorly understood. In the bone microenvironment, prostate metastatic foci are associated with the hematopoietic stem cell niche [6,7] and can remain dormant for extended periods. In this context, the endosteal layer of quiescent osteoblasts induces the dormant phenotype via several mechanisms [8,9]. Relevant to the present study, this bone microenvironment is the primary repository of calcium, which is incorporated and mobilized from the osteoid matrix to respond to systemic demand (reviewed in [10,11]). Factors like race [12], age [13,14], and concomitant morbidities like diabetes [15–18] negatively impact this bone calcium homeostasis resulting in osteopenia (loss of calcified bone mineral density) and osteoporosis (loss of mineral density that results in decreased bone strength). Adding complexity to these phenotypes, the standard of care for prostate cancer also negatively impacts bone matrix integrity. Specifically, androgen deprivation therapy (ADT: chemical castration, testosterone blockade) interferes with osteoblast homeostasis resulting in loss of mineral density [19,20]. These events could create a perfect storm of a microenvironment rich in bioavailable calcium which could influence cell proliferation (reviewed in Ref. [21]), and abnormal cell survival and apoptosis [22,23]. Critically, previous studies have shown that about fifty percent of patients who fail ADT therapy and develop castration-resistant prostate cancer (CRPC) will experience bone metastasis as well [24].

The role of bioavailable calcium in prostate cancer bone metastasis progression and the development of CRPC is poorly understood. In this study, we present the development of a cell culture system that incorporates an amorphous calcium phosphate coating to model the interactions of prostate cancer cells with this type of microenvironment.

Unfortunately, the COVID-19 pandemic placed an unusual strain on the supply chain of polypropylene-derived plastics necessary for research [25,26]. As a result, the production of cell culture specialty vessels like those needed to model the bone microenvironment was severely impacted. Spurred by this uncertainty in sourcing material for our studies, we set out to modify an amorphous calcium phosphate (ACP) chemical deposition system, originally developed to coat titanium for use on bioimplants [27]. Our system is useful for depositing amorphous calcium phosphate on untreated plastic cell culture vessels and glass coverslips. The technique is cost-effective, modular, and robust and can generate hundreds of cell culture plates in a few weeks, ensuring continuity of research independent of supply issues. Here we describe the advantages and challenges of the system, along with the methods developed for culturing prostate cancer cell lines on these surfaces and deriving viable biological samples from them.

Culturing normal (RWPE), adenocarcinoma (LNCaP), and bone metastatic (VCaP, MDAPCa2a) prostate epithelium on these ACP-coated vessels, we observed high cell attachment to calcium-rich surfaces and an induction of proliferation. We further identified changes in the transcription of genes related to cell proliferation and metastasis progression. Intriguingly, the presence of calcium compensated for the absence of testosterone in some cases, providing new insight into an alternative mechanism for the rise of castration resistance.

2. Results

2.1. Alkali-treated titanium catalyzes amorphous calcium phosphate aggregate formation and a surface for coating

To develop a cell culture system in which prostate cancer cells interact with a high bioavailable calcium microenvironment, similar to the metastatic bone site, we implemented a modified version of the amorphous calcium phosphate (ACP) coating on alkali-treated titanium as previously described [27]. We scaled the protocol to activate and coat multiple titanium plates of larger sizes, amenable for cell culture in 6 well plates (Fig. 1A). Activating the titanium surfaces in 5 M potassium hydroxide results in mild etching of the plate surface, evident under scanning electron microscopy (SEM) (Fig. S1 A-B). Incubation of these activated surfaces in ACP solution results

in aggregate formation, visible on the supernatant of the solution, as early as 24 h after the start of the coating phase (Fig. 1B). Replacing two-thirds of the solution every 24 h allowed for less disturbance of the coating surface and faster nucleation of the new solution, resulting in a white, chalky coating after four days of incubation (Fig. 1C), which persists after washing with chemically pure water. An evaluation of the coating using SEM confirms an amorphous, filamentous structure similar to that previously reported (Fig. 1D) [28,29].

2.2. X-ray diffraction analysis of ACP aggregates

The material deposited onto three ACP-coated glass coverslips, and 500 mg of ACP precipitate, collected from eighteen Petri dishes that were coated and then scraped as described in the methods section, were evaluated via X-ray diffraction. The three glass-coated

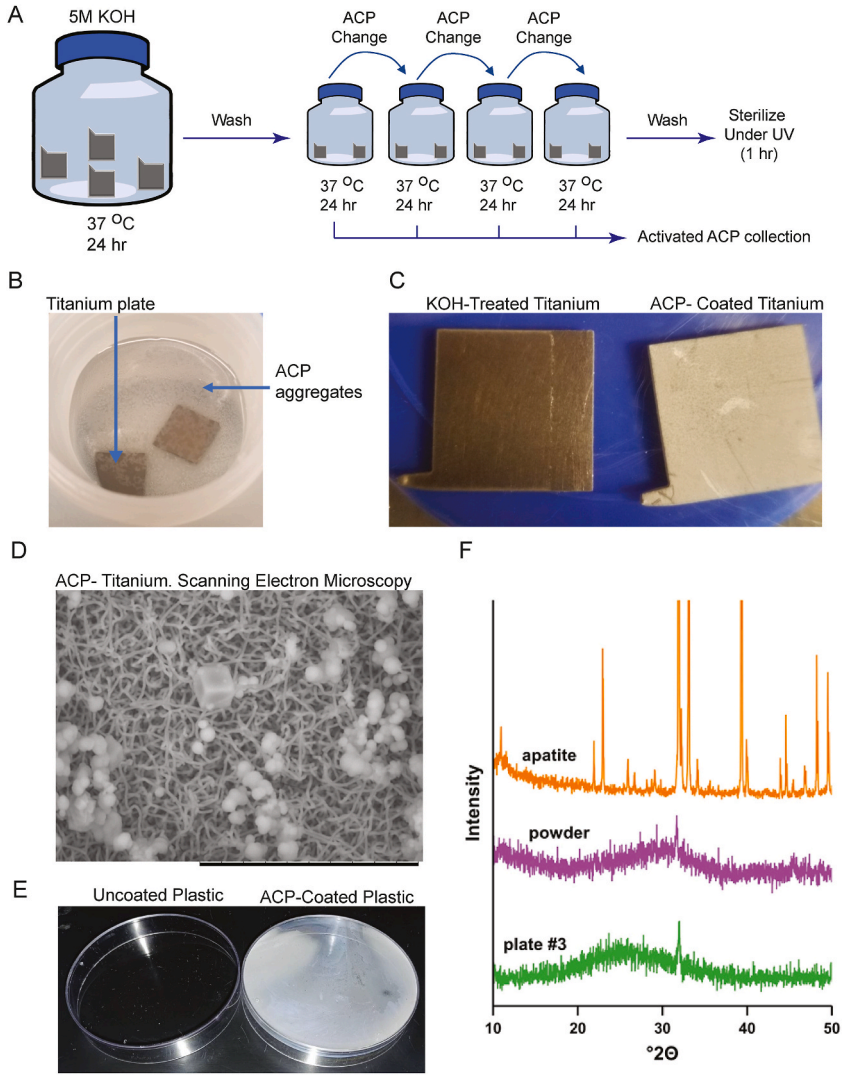

Fig. 1. Coating of potassium hydroxide-activated titanium plates with amorphous calcium phosphate (ACP) A. Graphic representation of the method for amorphous calcium deposition (ACP) on titanium surfaces and collection of activated ACP solution for plastic coating B. Incubation of potassium hydroxide-activated titanium plates with ACP solution for 24 h is enough to elicit nucleation of precipitate in the solution. C. Potassium hydroxide-activated titanium plates conserve a metallic sheen (left), while plates exposed to ACP solution for four days are coated with a persistent, white, chalky substance (right) D. Scanning electron microscopy shows that ACP-coated titanium plates are coated with a combination of amorphous globular structures and a fibrillar-like network (scale: 20 μm). Sodium chloride crystals are also observed, interspersed among those structures (cuboidal structure). E. ACP coating is persistent on non-treated plastic surfaces. ACP-coated plate (right) shows characteristic white powdered deposition compared to control plates incubated in buffer (left). F. X-ray diffraction (XDR) analysis reveals two peaks in the powdered ACP collected from petri dishes (purple- "powder"): a weak peak at 31.67 °2θ (d = 2.79 Å) and a weaker peak at 45.5 °2θ (d = 1.99 Å), while the sample coated on glass coverslips (green- "plate #3") shows profiles of a single weak diffraction line (peak) at 31.90 °2θ (d = 2.81 Å). The graph compares the XRD profiles of the unknown precipitates to that of apatite.

coverslips generated similar XRD profiles (Fig. 1E – green); these profiles consisted of a single weak diffraction line (peak) at 31.90 °2θ (d = 2.81 Å). The powder sample (Fig. 1E – Purple) generated two peaks: a weak peak at 31.67 °2θ (d = 2.79 Å) and a weaker peak at 45.5 °2θ (d = 1.99 Å). Fig. 1F compares the XRD profiles of the unknown precipitate to that of hydroxyapatite. Based on the XRD analysis, the only crystalline substances in the samples are KCl and NaCl. The bulk of the precipitate appears to consist of an amorphous

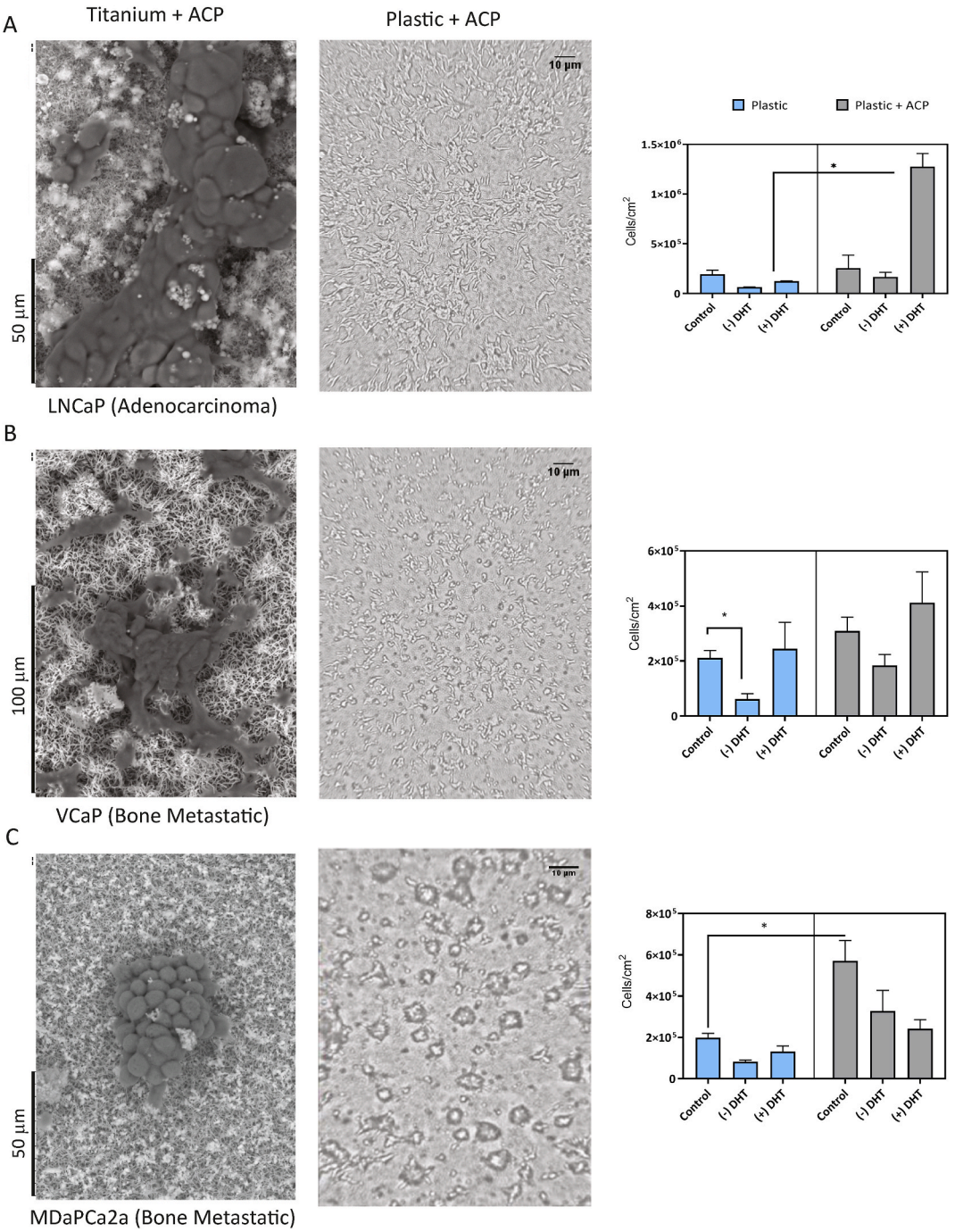

Fig. 2. Epithelial cell culture on ACP-coated, non-adhesive plastic surfaces Cell culture results are shown for Prostate adenocarcinoma cell line LNCaP (A), Bone metastatic prostate cancer cell line VCaP (B) and Bone metastatic prostate cancer cell line MDAPCa2a (C) grown on amorphous calcium phosphate surfaces. For each cell line: left panels show scanning electron microscopy of cells grown in ACP-titanium coated surfaces, bar 50 µm. Middle panels show cells cultured on ACP coated-non adhesive plastic for 48 h. Right panels show cell culture yield from full media control, testosterone depleted (-DHT), or testosterone supplemented (+DHT) conditions, in either standard tissue culture treated plastic (blue) or ACP coated plastic (grey). Unpaired *t*-test with Welch's correction * $p < 0.05$.

(microcrystalline) substance, similar to amorphous calcium phosphate reported in the literature.

2.3. Activated ACP solution can be used to coat plastic and glass cell culture vessels

Cells grown on titanium surfaces cannot be studied with light microscopy, so to enhance the utility of our ACP coating for a variety of downstream experiments, we next devised a way to use the ACP solution to coat plastic vessels. To evaluate how prostate cancer cells interact with calcium-coated surfaces, non-cell culture-treated plastic vessels were coated with activated ACP solution immediately after the four-day pooling from the titanium coating phase. We used bacterial culture Petri dishes, non-treated six-well plates, or glass coverslips to prevent confounding adhesion interactions with treated plastics. Treatment with ACP for four days at 37^{o}C is enough to coat both types of plastic (Fig. 1E) or glass (Fig. S1C). This coating is persistent after washing in chemically pure water, with vigorous shaking. Based on the collection of ACP precipitate used for the X-ray diffraction studies, and given that the coating appears to be homogeneous, we estimate that each 10-cm plate is coated with about 27 mg of ACP or about 0.4 mg/cm^2.

As described in the methods, sterilization under ultraviolet light does not affect the ACP structure or coating and is sufficient to prevent contamination during cell culture.

Petri dishes coated in ACP were incubated in standard full media formulations used for prostate cancer cell lines (Table S1) to verify the stability of the calcium phosphate coating during cell culture. We find that chemically defined media that does not contain serum (KSF) can strip a significant amount of ACP from the surfaces. To further evaluate changes in calcium concentration in the media, media pooled from four-day incubation on ACP-coated surfaces were submitted to ion chromatography analysis at the Water Quality Core Facility of the University of Tennessee, Knoxville. These results (Fig. S1D) confirm the visual observation of ACP stripping in KSF. Some increase in calcium concentration occurred on HPC1 media, with the coating still visible under the microscope. The consistency of the coating was confirmed by scraping the deposited ACP into a suspension in chemically pure water, followed by drying of the precipitated pellet. We confirmed that the deposited ACP among batches is consistent, between 6 and 7 mg of ACP per plate (Fig. S1E).

2.4. Culturing prostate cancer cell lines on ACP-coated surfaces fosters their adhesion, proliferation, and independence from androgen depletion

We cultured the adenocarcinoma cell line LNCaP and bone metastatic cell lines VCaP (White-European) and MDAPCa2a (African American) on ACP-coated titanium plates and plastics to evaluate the influence of an environment rich in bio-available calcium on prostate cancer epithelium.

The adenocarcinoma cell line (LNCaP) attaches readily to the ACP-coated surfaces (Fig. 2A). Cell viability is not affected by culturing on ACP surfaces, but the presence of both ACP and testosterone (DHT) supplementation increases proliferation (Fig. 2A, right). Strikingly, LNCaP cells cultured in ACP-coated vessels are not sensitive to the absence of testosterone modeled using charcoal-dextran-treated serum in the culture media. After four days of culture on tissue culture treated plastic and charcoal-dextran serum conditions, we observe a well-documented decrease of LNCaP proliferation, while cells proliferate at the normal rate on ACP-coated plastic. The cells do not adhere to the untreated plastic without ACP coating, even in the presence of an equivalent amount of additional free calcium in the media, indicating this cell attachment phenotype is a surface coating-dependent effect (Fig. S1G).

The bone metastatic cell line VCaP adheres readily to ACP surfaces. (Fig. 2B). VCaP cells show a prototypical response to the absence of testosterone in normal plastic at four days, with a significant proliferation decrease when cultured in media containing charcoal dextran-treated serum. This effect is rescued by the addition of testosterone to the media. Similarly, to our observations in LNCaP, culturing the VCaP cell line on ACP-coated surfaces bypasses the proliferation arrest that results from the absence of testosterone (Fig. 2B right).

In contrast to the other cells used in this study, the bone metastatic cell MDAPCa2a cannot adhere to cell culture-treated plastics unless coated with a mixture of fibronectin and collagen (FNC coating - Athena biologicals). Growing on this extra-cellular matrix protein context and at the 4-day experimental timepoint, MDAPCa2a cells show a small proliferative decrease when cultured in media with charcoal dextran-stripped serum. This proliferation decrease, as in VCaP, is rescued by the addition of testosterone. Strikingly, MDAPCa2a culture on ACP-coated surfaces (titanium and plastic) does not require FNC coating. Cells adhere to the surface, making both the characteristic 3D colonies observed in plastic, with single cells growing in a monolayer as well (Fig. 2C). Further, these cells show a similar trend as VCaP regarding the presence and absence of testosterone in plastic (Fig. 2C right). The presence of the ACP surface results in a significant increase in the proliferation of MDAPCa2a cells in the presence of complete media. In contrast to VCaP cells, however, MDAPCa2a cells show a non-significant decrease in proliferation when cultured in media containing charcoal-dextran-treated serum. Interestingly, this effect is not rescued by the addition of testosterone, suggesting that the absence of another steroid-like compound present in the serum could affect the proliferation of these cells (Fig. 2C right).

Cells cultured on ACP in charcoal dextran stripped (testosterone depleted) serum show nuclear localization of androgen receptor. The number of nuclear AR-positive LNCaP cells cultured on ACP does not change, regardless of the presence of testosterone in the media, however, there is a significant increase in AR-positive cells observed in VCaP (Fig. S4A). This AR localization is accompanied by differential transcriptional regulation of AR-regulated genes, like PSMA1 and PSMA6, among others (Fig. S4B).

2.5. Culture in ACP-coated surfaces results in an altered transcriptional landscape

To evaluate the transcriptional effect that bioavailable calcium coating has on prostate epithelial cells, we collected RNA from our model cell lines (RWPE, LNCaP, VCaP, and MDAPCa2a) cultured under different conditions: cell culture-treated plastic or ACP-coated

non-cell culture treated vessels were used in combination with control media, media without testosterone (using charcoal-dextran stripped serum), or media supplemented with testosterone (in charcoal-dextran stripped serum). We found that RNA quantity and quality remained high when isolated from cells grown on ACP surfaces (Fig. S1F) enabling the generation of RNA-seq libraries from all samples.

Two unsupervised analyses were used to compare the transcriptomic output of each of these experimental conditions. First, genes that showed a log2 fold change with a cutoff of ± 1 for each condition were analyzed using Metascape to find enriched biological pathways and functions [30] (full gene lists and enrichment results are available in Data S1). In agreement with our proliferation data, this analysis revealed that three main functional categories are enriched for transcriptional upregulation when non-tumorigenic (RWPE) or early adenocarcinoma (LNCaP) cell models are grown in contact with calcium surfaces: Cell cycle progression (Fig. 3A, Table S2), oxidative phosphorylation (Fig. 3B–Table S2) and translation/ribosome assembly (Fig. S2). Genes common to these ontologies and comparisons include CDK1, COMMD3, B2M, CDK7, and COX17.

Further, to assess whether common genes were affected in different cell lines treated in the same conditions, we intersected gene lists that showed a significant change (FDR p-adjusted value < 0.001). We find that fifty-two genes upregulated by culturing RWPE on calcium-rich surfaces are further upregulated when culture on calcium is supplemented with testosterone (Fig. 3C). Sixty-three genes that are upregulated in normal epithelium cultured on calcium are also upregulated in adenocarcinoma cell lines under the same condition (Fig. 3D). Genes common to these comparisons include CDK1, PARPBP, ANKRD22, ITGAE, and COX7B. Only fourteen genes are common among the normal epithelium-bone metastatic cell line comparison (Fig. 3E–Table S3). Full gene expression profiles of these and other prostate cancer progression related genes are shown in heatmaps in Fig. S3.

Finally, we evaluated whether transcription of genes whose expression increased in the context of our experimental bioavailable

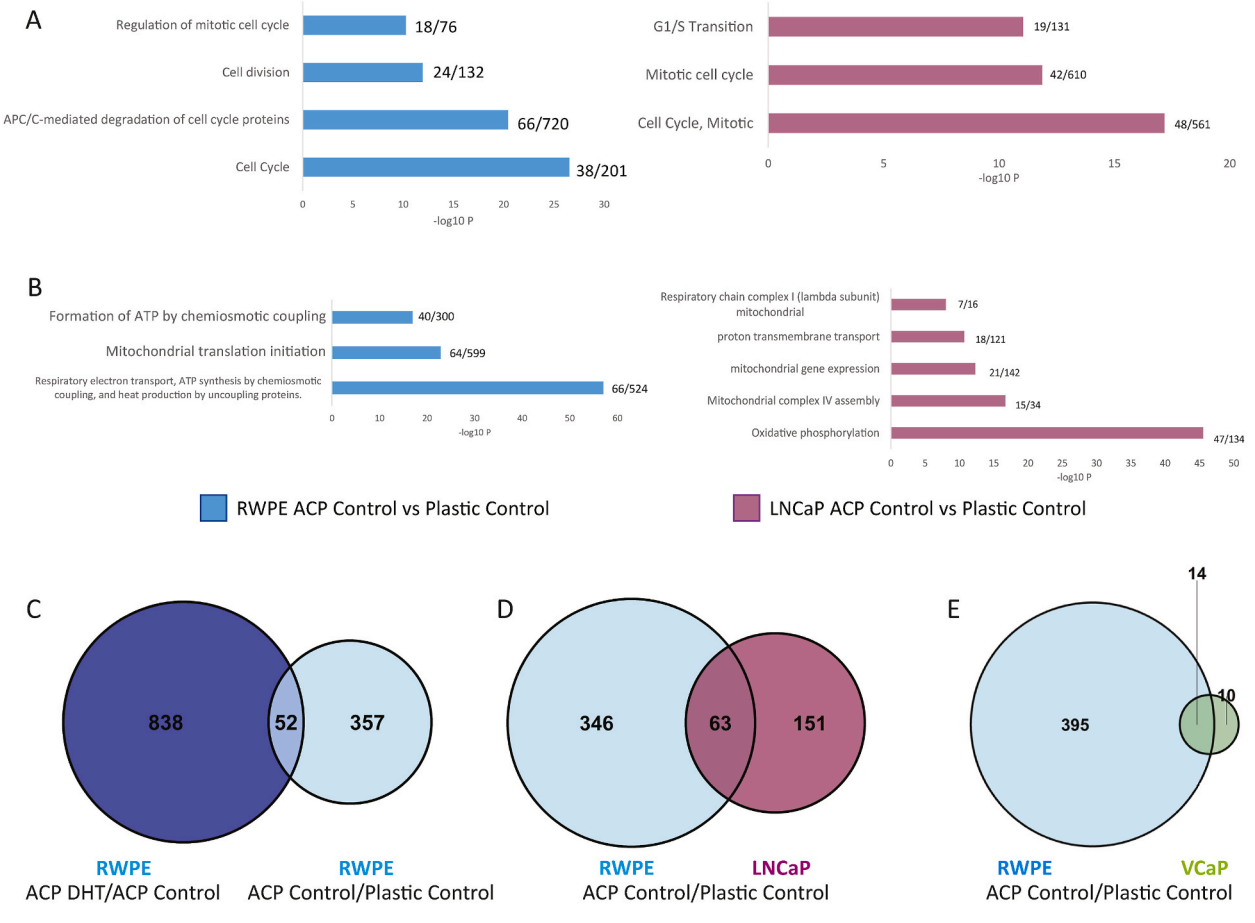

Fig. 3. Congruent changes in transcription are observed in prostate non-tumorigenic epithelium and adenocarcinoma cells cultured on ACP surfaces. A. Culturing the non-tumorigenic cell line RWPE (left) and the early adenocarcinoma cell line LNCaP (right) on calcium-coated surfaces induces transcription of genes related to cell cycle progression when compared to culture in normal plastic (Full gene list in Table S2). B. Culturing RWPE and LNCaP on calcium-coated surfaces induces transcription of genes related to oxidative phosphorylation (Full gene list in Table S2). C. The addition of testosterone to RWPE culture on calcium-coated surfaces further enhances transcription of a cohort of 52 genes. D. Comparison of transcriptionally upregulated genes common between normal epithelium (RWPE), adenocarcinoma (LNCaP) and (E) bone metastatic cell (VCaP) line, shows common hubs of genes that are upregulated in calcium-rich culture conditions (Gene lists: Table S3, expression profile heatmaps: Fig. S3).

calcium model also increased in patients by analyzing available prostate data from The Cancer Genome Atlas (GDC TCGA PRAD). This cohort includes data from six hundred and twenty-three patients (81 % tumor samples, 19 % normal samples). Using data from patients with a reported Gleason score, we find that CDK1 and DEPDC1B high expression is upregulated in tumor samples (Fig. S5A) and correlates with biochemical recurrence (Fig. S5B). The expression of these genes also correlates with a higher Gleason Score and is concurrent with each other as the Gleason Score increases (FigS5 C-D).

3. Discussion

Advanced prostate cancer metastasizes preferentially to the bone [31]. Importantly, at the time of diagnosis, about a quarter of all prostate cancer patients already present with tumor-circulating cells (reviewed by [5,32]), that might arrive at the bone niche through circulation, remaining in a dormant state under the influence of osteoblast-secreted signals [8,33].

Previous studies have characterized a reactive, fracture repair-like endosteum associated with trabecular prostate cancer metastasis [34] and the important role of bone calcium in the context of cancer [35]. These two separate observations can be intimately related since the processes of bone remodeling, via deposition of new osteoid by osteoblasts or bone matrix degradation mediated by osteoclasts, play an important role in the release of bioavailable calcium (reviewed by [36]).

The present work established a cell culture system with a solid-phase bioavailable calcium coating to model a receptive bone microenvironment. In this context, bioavailable calcium is defined as A) calcium that is compatible with body fluids and is present in native tissues in solid form, B) fosters biological activity by mediating adhesion and proliferation, and C) a matrix that can be degraded by cells and release calcium ions [37]. Specifically, amorphous calcium phosphate (ACP) coatings are biologically relevant since they foster new bone formation by osteoblasts, inducing faster mineralization and osteogenic induction [28]. ACP also enhances MSC-mediated reconstruction of bone defects and engraftment [38] and increases titanium implant biocompatibility and bonding strength, even in the presence of coating resorption [39].

Further, it has been proposed that ACP acts as a potential intermediate in the precipitation of hydroxyapatite *in vitro* [40,41]. While there is controversy about the presence of non-crystalline phase apatite and amorphous calcium phosphate in bone [42], several studies have characterized disordered calcium phosphate deposition. Amorphous calcium compounds are predominant in new segments of ray bones in zebrafish [43], where they act as precursors of the mature bone's carbonated hydroxyapatite. Further, a detailed transformation mechanism of amorphous calcium phosphate particles into apatite-like crystals has also been described within the confined domains of a fibrous nanocomposite resembling the collagen matrix in the developing bone [44]. Conflicting studies that characterized the absence of amorphous calcium phosphate content in bone [45] were hindered by a limited sample size of two adult cadaveric donors since ACP deposition is more prevalent in young vertebrates [46].

Our ACP coating, modified from established protocols based on alkaline-treated titanium catalysis [27], allows the coating of large surface-area cell culture vessels onto otherwise non-adhesive plastic. This is a critical advantage to commercially available materials currently limited to small well formats. The method requires simple equipment (ovens, shakers, mixers) and cost-effective reagents that are broadly available, making it accessible. This ACP formulation creates a resilient solid phase in otherwise non-adhesive cell culture plastics, stabilized by serum-containing media. We recommend caution using this system in non-serum-containing experiments, since chemical-defined media results in calcium release from the matrix into the liquid phase of the culture. These higher calcium levels could be toxic for non-prostate epithelial cell lines. While the system is limited to in-vitro modeling and represents only one physical phase of calcium present in the bone, it lends itself to modifications such as the incorporation of secondary coating with extracellular matrix proteins or the development of co-culture bone cells (osteoblasts, osteoclasts), making it a modular solution to query the complex bone microenvironment.

All prostate epithelial-derived cells used in this study showed a high binding affinity to the ACP-coated surfaces, and enhanced proliferation, even when cultured in media supplemented with charcoal-dextran stripped serum, as a model for androgen depletion. These results are critical since androgen deprivation therapy (ADT) remains the standard for localized prostate cancer therapeutic care. As the tumor recedes after the initial interventions, residual disease can proliferate again, eliciting sequential patient exposure to ADT [47]. Unfortunately, some patients develop tolerance to treatment and evolve into a castration-resistant phenotype (CRPC) (reviewed by [48], and [49]). Our results carry the dangerous implication that interaction with bioavailable calcium is sufficient to elicit androgen independence, which could mediate, in part, the rise of castration resistance. Hormonal ablation has a well-characterized side effect of bone loss, with a substantial increase in bone fractures in patients with recurrent ADT exposures [47,50]. Further, factors related to worsening bone health are the primary indicators of poor prognosis associated with bone metastasis [51–53]. We propose that subclinical fractures resulting from therapy exposure activate the bioavailable calcium pool in the metastatic niche, and, through undefined mechanisms, allow retention of the androgen receptor inside the nucleus, even in the absence of testosterone, helping the progression into CRPC. Further, our observations are concordant with recent findings showing that treatment of AR-positive prostate epithelium with soluble calcium increased androgen-mediated cell proliferation and the expression of androgen-regulated genes [54].

In agreement with our enhanced proliferation observations, ACP-coated culture elicits transcriptomic induction related to cell cycle progression, oxidative phosphorylation, and transcriptional elongation in both non-tumorigenic and early-adenocarcinoma prostatic epithelial cell lines (RWPE and LNCaP, respectively). Further evaluation of these genes against the Cancer Genome Atlas dataset for prostate cancer (PRAD) revealed that CDK1 and DEPDC1B expression is concomitant, correlating with a higher incidence of biochemical recurrence and increased Gleason score, which in turn signals a potentially poor prognosis.

4. Conclusions

Recent understanding of the importance of bone health in preventing metastatic progression and improving patient outcomes has given rise to combination therapies that foster bone homeostasis [20,55,56]. However, molecular changes during prostate cancer progression and the subsequent rise of treatment resistance should influence therapy choice [57]. The ACP-coating system developed in this study is cost-effective and scalable and a simple way to incorporate bioavailable calcium in studies that require modeling the osteogenic bone niche. Finally, our results revealed that an environment rich in calcium is enough to rescue prostate epithelial cells from androgen removal *in vitro*. Our findings highlight the importance of including calcium as a confounder to Androgen Receptor biology in the study of castration-resistant prostate cancer and a critical need to incorporate biologically relevant models that mimic the reactive bone microenvironment in the study of prostate cancer metastasis.

5. Methods

5.1. Titanium plates

Titanium Foil, 0.89 mm thick, 99.7 % metal basis (Alfa Aesar, AA10399GW) was cut into 2 × 2 cm plates, using an OMAX2626 JetMachining Center. A small triangular tab was included in the upper left corner of the design to facilitate identification and orientation of the activated/exposed surface during coating.

5.2. ACP coating

5.2.1. Titanium plates

Coating of titanium surfaces was performed according to Ref. [27] with modifications. Briefly, activation of the titanium surface was achieved by incubating four titanium plates (16 cm^2 total surface area) in 500 ml of potassium hydroxide, at 37°C, inside a tightly closed, 1-L, polypropylene bottle (Nalgene, 75007300), for 24 h.

After surface activation, bearing in mind to keep hydroxide-exposed surfaces up, plates were washed in three changes of milliQ water, 20 ml each, for 5 min under orbital shaking. Plates were then transferred, in pairs, to clean, 1-L, polypropylene bottles for ACP deposition.

The ACP solution was prepared in 1-L batches. Using eight hundred milliliters of MilliQ water under constant magnetic stirring as the solvent, each reagent was added in a stepwise manner, allowing it to dissolve fully before adding the next one. (Refer to Table S4 for the detailed formulation, as per Kim et al. [27]). Sodium chloride was added first, followed by potassium chloride, magnesium chloride (hexahydrate), calcium chloride (dihydrate), sodium bicarbonate and sodium phosphate (dibasic, hydrate). The sudden addition of the reagents, or an alteration of the order, caused premature precipitation. After all the reagents were dissolved, the solution was transferred to a graduated cylinder and the volume was adjusted to 1 L with MilliQ water. Nine hundred milliliters of freshly made ACP solution were added to each of the polypropylene bottles, containing two titanium plates, activated side up (total surface area 8 cm^2). Bottles were tightly closed and incubated in a 37°C oven for 24 h. After the 24-h incubation, two thirds of the ACP solution was collected from the incubation chambers and replaced with freshly made solution. This process was repeated two more times, for a total of 4 days incubation. All ACP solution was pooled together (Activated ACP), for usage in the coating of glass and plastic cell culture vessels.

After the four-day incubation, titanium plates were removed from the chamber, washed with an excess of milliQ water, for 30 min, under orbital shaking, and allowed to air dry for at least one day before sterilization (Fig. 1A). Coating was verified as a white, powder deposit, and via SEM of each batch.

5.2.2. Bacterial plates

Activated ACP solution was added to plastic vessels that are non-adhesive to mammalian cells such as plastic petri dishes (Fisher brand FB0875713. 15 ml per plate), or non-treated 6 well plates (VWR 10861-554. 5 ml/well) and incubated for four days in a 37°C oven. After incubation, ACP solution was aseptically removed and collected for filtering, while plates were washed with an equivalent volume of milliQ water, with orbital shaking, for 30 min. Coating was visually verified as a white powder deposit.

Deposited ACP was collected from 10-cm, petri dishes to verify the consistency of the coating. Briefly, 100 μL of chemically pure water were added to a plate and the ACP was carefully scraped from the surface using a lifter blade scraper (Celltreat, 229316). The 100 μL were collected once saturation was reached and new water was added in 100 μL aliquots, repeating the scraping steps until the plate surface appeared clean. About 500 μL of ACP suspension were collected in total for each plate. Powdered ACP was washed with absolute ethanol by centrifugation at 13000 rpm for 10 min at room temperature to remove moisture, and allowed to air dry before measuring the mass collected.

5.2.3. Glass coverslips

Square glass coverslips were flame-sterilized inside the biosafety cabinet, and installed in six well-plates, one coverslip per well. Coverslips were washed twice with 5 ml of PBS, and allowed to thermally stabilize inside a 37°C, 5 % CO2 incubator for at least an hour prior to usage. For ACP coating, PBS was removed, and substituted with 5 ml of activated ACP, per well. Plates were then incubated in a 37°C oven for four days. After ACP incubation, plates were washed with three, 10-min incubations in sterile milliQ water (5 ml each).

All ACP-coated vessels were sterilized under ultraviolet light, inside a biosafety cabinet, for 2 h and stored in sterile polypropylene

zip lock bags until use.

5.2.4. Activated ACP disposal

Activated ACP precipitates readily and is pervasive on most plastic and glass surfaces. The high nucleation efficiency of ACP could have a deleterious effect in the water supply and increase mineral deposition in water lines. For this reason, activated ACP was filtered through 0.2-μm membranes (Corning 430769), which significantly reduces the amount of salt aggregates in the solution, before disposal.

5.3. X-ray diffraction (XRD) analysis

Deposited ACP was collected from 10-cm, petri dishes as previously described, pooling the ACP from 16 plates. The powder (yield 97 mg) was allowed to air dry overnight before X-ray diffraction analysis.

X-ray diffractograms were generated using random powder mounts and a Brüker Model D8 with Ni-filtered, Cu Kα radiation. The x-ray diffractometer operating parameters were set to 40 kV and 40 mA with a scan range of 10–50° 2θ, and a count rate of 2 s per step. XRD analysis was performed on three ACP-coated glass coverslips and on powdered ACP, scrapped from 20 coated petri dishes. Glass coverslips were analyzed by placing them directly into the XRD instrument. The powder was suspended in water and the suspension deposited on a glass slide (creating a powder mount). After drying, the slide was placed into the XRD instrument and analyzed. Powder mounts of the mineral apatite and reagent grade NaCl (halite) were also analyzed as controls.

5.4. Cell culture

A cohort of prostate epithelial cell lines was selected to represent stages of prostate cancer progression: immortalized normal epithelium (RWPE), early adenocarcinoma (LNCaP), and bone metastasis (VCaP of Caucasian ancestry and MDAPCa2a, derived from an African American patient).

RWPE (Normal epithelium, RRID:CVCL_3791) [58], LNCaP (early adenocarcinoma, RRID:CVCL_1379) [59] and VCaP (bone metastatic, RRID:CVCL_2235) [60] were obtained from ATCC (Cat. No CRL-11609, CRL-1740 and CRL-2876, respectively), through the Physical Sciences Oncology Network Bioresource Core Facility. All cells were cultured in T75 filtered flasks (Corning 430641U). RWPE was cultured in keratinocyte SFM, supplemented with EGF and bovine pituitary extract (Gibco 17005042), and sub cultured by incubation for 2 min in 1 ml of 0.25 % Trypsin-0.53 mM EDTA (Gibco, 25200072) at 37°C, followed by neutralization with defined trypsin inhibitor (Gibco R007100) to a ratio of 1:20 enzyme to inhibitor. LNCaP media was composed of RPMI (Gibco, 11875119) supplemented with 10 % FBS (Corning 35-010-CV), glucose (Corning, 25037CI), HEPES (Gibco, 15630080) and sodium pyruvate (Gibco, 11360070) to match the concentrations suggested by ATCC (4.5 g/L glucose, 2.383 g/L HEPES and 0.11 g/L sodium pyruvate). Media used for VCaP culture was 10 % FBS, in DMEM: F12 Ham 1:1 basal media.

MDAPCa2a cells (RRID: CVCL_4747)were a kind gift from Dr. Nora Navone (MD Anderson Cancer Center, Houston TX) [61]. Cells were cultured in the same type of T75 vessel, coated with FCN coating mix (Athena Biologicals Cat. No. 0407), according to the manufacturers' protocol. Media for MDAPCa2a cells was composed of BRFF-HPC-1 base media (Athena Biologicals Cat. No. 0403), supplemented with 20 % FBS.

All cell culture media was supplemented with 1X penicillin/streptomycin (Gibco 15140122). Media formulae as described were used for culture in ACP-coated surfaces.

All cell lines tested negative for mycoplasma using a PCR assay (Biovision/Abcam) and were authenticated via STR testing (ATCC).

For trypsinization from ACP-coated petri dishes (10 cm), media was aseptically removed, and the cell monolayer was briefly rinsed with 5 ml of 5 mM EDTA solution in HBSS. Cells were then exposed to a brief trypsin wash using 0.25 % trypsin - 0.53 mM EDTA (Gibco), supplemented to a final EDTA concentration of 1.3 mM. Cells were further incubated in another aliquot of EDTA-supplemented trypsin for 2 min in a 37°C, 5 % CO_2 incubator. After incubation, with trypsin still on the plate, plates were vortexed for 15–20 s, using a Vortex Genie equipped with a flat surface adaptor (setting No.3). Enzymatic dissociation was then neutralized by adding 7 ml of full media, followed by centrifugation (5 min, 800×*g*). Viability and cell number was evaluated via trypan blue exclusion using a CytoSMART cell counter. This protocol was used for both subculture, and RNA-protein sample collection.

5.4.1. In-vitro androgen treatment

For supplementation of androgen in our cell culture experiments, a batch of BRFF-HPC-1 base media (Athena Biologicals) was purchased, custom-made to a final concentration of 0.5 μg/ml of dihydrotestosterone and used as stock solution. Complete media for LNCaP, VCaP and MDAPCa2a was prepared as previously described, substituting FBS with an equivalent volume of HyClone charcoal/dextran treated FBS (Cytiva/HyClone Cat.No. SH30068.03). 2.9 ml of modified BRFF-HPC-1 media was added per 50 ml of total media for a final DHT concentration of 100 mM (media formulation referred to as "DHT +"). An equivalent volume of BMZERO media (Athena Biologicals Cat. No. 0401) was used to supplement negative control media (media formulation referred to as "DHT -"). Media containing normal FBS is referred to as "DHT Control".

Given that the RWPE cell line grows in serum-free media, for these cell lines the only supplementation necessary was modified BRFF-HPC-1 media or BMZERO control, as previously described.

5.4.2. Cell culture on titanium plates: sample preparation for electron microscopy studies

Five hundred thousand cells (VCaP, LNCaP) were seeded per sterile ACP-coated titanium plates, housed in non-treated 6 well

plates, using 5 ml of cell-specific media. Cells were cultured for 4 days, with a change of media at 48 h. Cells were fixed *in-situ* by removing 2 ml of media and adding 3 ml of 8 % paraformaldehyde (Alpha Aesar, 473479M), for a final concentration of 4 %, and incubated for 20 min at room temperature. After fixation, the media/fixative was removed and plates were washed three times in 5 ml of sterile PBS, under orbital shaking. Plates were then dehydrated in a series of graded ethanol (three washes each of 70 %, 95 %, 100 %), and allowed to air dry.

5.5. RNA purification and RNA-seq

RNA was purified from five million-cell pellets, using the Rneasy Plus kit (Qiagen, 74034), according to the manufacturer's instructions, using the RLT lysis buffer supplementation with β-mercaptoethanol, as suggested. Samples were homogenized using QiaShredder columns (Qiagen, 79656), before genomic DNA removal and purification steps. RNA quality was assessed using a NanoDrop spectrophotometer.

RNA-seq was performed by Genewiz (South Plainfield, NJ) using PolyA selection for mRNA species.

5.6. RNA-seq data processing. Differential expression analysis and gene ontology

RNA-seq data was processed according to previously reported pipelines. Briefly, fastq files were processed with BBDuk tool (https://github.com/kbaseapps/BBTools), trimming adapters (ktrim = r k = 23 mink = 11 hdist = 1), and low quality reads (lower than 28: "qtrim = r trimq = 28"). The reads were then aligned to the reference genome hg19 using STAR aligner (https://github.com/alexdobin/STAR) with ('–outFilterScoreMinOverLread' and '–outFilterMatchNminOverLread' parameters set to 0.2). Mapped reads were arranged via their genomic coordinates and feature counts generated with HTSeq-Counts (https://github.com/simon-anders/htseq).

Differential gene expression analysis between experimental conditions was evaluated using DESeq2 (https://bioconductor.org/packages/release/bioc/html/DESeq2.html) and genes defined as up/down regulated for each of the comparisons, were considered for gene ontology analysis based on a log2 fold change higher/lower than a factor of 1. Gene lists were analyzed using Metascape [30]. Full gene lists and enrichment results are available in Data S1. Gene ontology results were analyzed for commonalities among comparisons. Finally, batch adjusted counts for genes of interest were log2 normalized with a pseudo count of 1. Gene expression was plotted as a heatmap per sample/condition using the Seaborn python package (https://seaborn.pydata.org/).

5.7. Protein collection and western blot

Pellets containing five million cells were collected by centrifugation at 1000*g* for 5 min. After removing the supernatant, pellets were lysed in 300 μl of RIPA buffer (Thermo Scientific 89900) containing protease/phosphatase inhibitors and EDTA (GenDepot, P3100001 and P3200001), incubating on ice, for 10 min 0.75 U of micrococcal nuclease (Thermo Scientific ENO0181) were added to each sample, and calcium chloride was added to a final concentration of 1 mM. Samples were then incubated for 15 min at 37°C, 15 min at 68°C, and on ice for 10 min, and stored at −20°C for a maximum of two weeks.

For Western blot, samples were thawed on ice and centrifuged at 14,000×*g* for 5 min at room temperature. The supernatant was transferred to a clean tube and the pellet was resuspended in 40 μl of 1X NuPAGE LDS sample buffer (Invitrogen NP0007) supplemented with DTT according to the manufacturers' protocol. Two hundred microliters of supernatant were concentrated by acetone precipitation, adding 800 μl of ice-cold acetone and incubating at −20°C for 2 h. Protein was collected by centrifugation at 14,000×*g* for 10 min at room temperature. The supernatant was discarded, and the pellet resuspended in 1X NuPage LDS buffer before electrophoresis.

All protein samples (membrane pellets, raw supernatant and acetone precipitated), were denatured at 70°C for 10 min, allowed to cool to room temperature and resolved using Bolt MES-SDS running buffer on NuPAGE 4–12 % Bolt Bis-Tris mini protein gels (Invitrogen, NW04127BOX) and further transferred to methanol-activated PVDF membranes (MilliporeSigma™ Immobilon™-FL PVDF, IPFL00010) using an Invitrogen Bolt Mini Module and Bolt Transfer Buffer (Invitrogen, BT0006). Transfer was conducted at room temperature, for 1 h, at 20 V.

Membranes were blocked with Intercept-TBS Blocking Buffer (LiCor 927–66003), for 1 h at room temperature and exposed to 15 ml of a primary antibody solution (Rabbit polyclonal to GAPDH, Abcam ab9485), prepared at a 1:2500 ratio (15 ml) on Intercept-TBS antibody diluent (LiCor 329–66003), overnight at 4 °C, with horizontal shaking. After three washes with TBST, membranes were then exposed to IRDye 680CW Goat anti Rabbit antibody (LiCor, 92668071, 1:20,000), for 1hr, prepared in the LiCor diluent, supplemented with 0.01 % SDS, in the dark with gentle shaking. After three washes with TBST (in the dark), membranes were imaged using an Odyssey CRx infrared scanner (LiCor).

We found that protein was not present in the acetone precipitated supernatant but that protein detection instead required solubilizing the membranous pellet, where the protein had aggregated due to the presence of excess calcium (Fig. S1H).

5.8. Scanning electron microscopy

ACP-coated titanium plates were imaged using a Hitachi TM3030 scanning electron microscope at an accelerating voltage of 15 kV, a working distance between 6800 and 7000 μm, at a magnification of x5000.

5.9. Evaluation of calcium leaching

Two ACP-coated petri dishes from at least three different ACP coating batches were incubated with 15 ml of full RWPE, LNCaP and VCaP media for four days, at 37°C, 5 % CO_2. After incubation, media was aseptically collected, pooled, filtered through 0.2-μm PVDF filters (low protein binding) and stored at −20°C. Samples were diluted 1:10 with chemically pure water before analysis.

Calcium leaching was measured at the University of Tennessee Water Quality Core Facility using ion chromatography (IC) using a Thermo-Scientific®/Dionex® ICS-1100 (cations) system with background suppression for low detection limits.

5.10. Immunocytochemistry

Cells (LNCaP and VCaP) were seeded on ACP-coated plates. In both cases, 6 well plates were seeded under control conditions (normal serum) and testosterone starvation (charcoal-dextran stripped serum), as described in the main text methods section. Media was replaced after overnight incubation. Cells were then cultured for four days, with a media replacement on the third day. All data represents two independent experiments, performed in cells from two different passage numbers.

Cells were fixed by adding 2 ml of 8 % paraformaldehyde (Thermo Scientific Chemicals 0473479M) to each well, incubating at room temperature for 20 min. Fixative was removed and the wells were then washed under gentle agitation three times, for 5 min each time, using PBS.

Staining was performed directly on the plastic surface. Cells were blocked and permeabilized at room temperature by incubation in PBS containing 10 % goat serum, and 0.5 % Triton, for 1 h. Wells were washed as previously described to remove the blocking buffer, before primary antibody incubation (Androgen Receptor: Bioss BSD0118E Rabbit Polyclonal 1:100 in 50 % blocking buffer/PBS, 500 μl per well). Primary antibody incubation was carried out overnight in refrigeration.

Wells were then washed as previously described before incubation in 500 μl of secondary antibody (Goat anti-Rabbit IgG (H + L) Cross-Adsorbed ReadyProbes™, Alexa Fluor 594 R37117), prepared according to the manufacturer's instructions, for 30 min.

After removal of the secondary antibody and washing, each well was briefly exposed to 500 μl of Vectashield Plus Antifade Mounting Medium with DAPI (Vector Labs H-2000), ensuring that all the cell monolayer was exposed to the non-hardening media, removing the excess by aspiration. Plates were preserved in refrigeration until imaging.

For this analysis, tiled images, representing two independent experiments, were captured at 10X magnification using an EVOS M7000 epifluorescence microscope. These tiles, a composite of 50 images on average represent 50 % of the total effective cell culture area, excluding the edges of the wells. Cell count per tile was determined using the Analyze Particles function in Image J on the DAPI channel and normalized per area of capture to determine the number of cells per square centimeter. Tiles for the DAPI and Texas Red single channels were analyzed using the JACOP plugin in Image J (v2.1.4), with calculations for Mander's Coefficients for red color overlapping blue, indicating nuclear AR.

5.11. Statistical analysis

Statistical analysis was performed using GraphPad Prism Software (v.10.3.1).

Calcium leaching and cell adhesion to ACP were analyzed using an unpaired *t*-test. Amorphous calcium phosphate coating efficiency among runs was tested using one-way ANOVA with Tukey's multiple comparisons.

AR localization in cells cultured on ACP in the absence of testosterone and TCGA data analysis related to expression of genes of interest relationship to Gleason Score were evaluated using one-way ANOVA, Kruskal-Wallis for multiple comparisons; TCGA data analysis regarding sample type and biochemical recurrence was analyzed using the Mann-Whitney test.

CRediT authorship contribution statement

Rebeca San Martin: Writing – review & editing, Writing – original draft, Methodology, Investigation, Formal analysis, Conceptualization. **Prijoyit Das:** Formal analysis, Data curation. **Tianchun Xue:** Software, Data curation. **Morgan Rose Brown:** Investigation. **Renata Dos Reis Marques:** Investigation. **Michael Essington:** Methodology. **Adrian Gonzalez:** Methodology, Investigation. **Rachel Patton McCord:** Writing – review & editing, Supervision, Resources, Project administration.

Ethics approval and consent to participate

The human cell lines used in this study are commercially available, commonly used for research and de-identified, therefore did not require ethics approval or consent.

Consent for publication

Not applicable.

Permission to reproduce material from other sources

Non applicable.

Clinical trial registration

Non applicable.

Data availability statement

All gene expression data for prostate cancer cell lines grown with and without testosterone on control and ACP surfaces are available at GEO accession number GSE227511 https://www.ncbi.nlm.nih.gov/geo/query/acc.cgi?acc=GSE227511.

Funding

This work was supported by National Institutes of Health NIGMS Grant R35GM133557 to R.P.M. R. San Martin was supported by a postdoctoral fellowship from the American Cancer Society (134060-PF-19-183-01-CSM).

Declaration of competing interest

The authors declare the following financial interests/personal relationships which may be considered as potential competing interests: Rachel Patton McCord reports financial support was provided by NIH National Institute of General Medical Sciences. Rebeca San Martin reports financial support was provided by American Cancer Society. Rachel Patton McCord reports a relationship with Cell Press that includes: board membership. If there are other authors, they declare that they have no known competing financial interests or personal relationships that could have appeared to influence the work reported in this paper.

Acknowledgments

The authors would like to acknowledge Jaydeep Kolape and the University of Tennessee Advanced Microscopy and Imaging Center for instrument use, and scientific and technical assistance with SEM.

Appendix A. Supplementary data

Supplementary data to this article can be found online at https://doi.org/10.1016/j.heliyon.2025.e41929.

References

[1] R.L. Siegel, A.N. Giaquinto, A. Jemal, Cancer statistics, 2024, CA A Cancer J. Clin. 74 (1) (2024) 12–49.
[2] G. Gandaglia, et al., Reply from Authors re, Improving outcomes from prostate cancer: unlocking the treasure trove of information in cancer registries. Eur Urol 2016;69:1013-4, in: Julia Verne, Luke Hounsome, Roger Kockelbergh, Jem Rashbass (Eds.), Eur. Urol. 69 (6) (2016) 1015.
[3] T. Todenhofer, et al., Microfluidic enrichment of circulating tumor cells in patients with clinically localized prostate cancer, Urol. Oncol. 34 (11) (2016) 483e9–483e16.
[4] L. Broncy, P. Paterlini-Brechot, Clinical impact of circulating tumor cells in patients with localized prostate cancer, Cells 8 (7) (2019).
[5] G. Theil, et al., In vivo isolation of circulating tumor cells in patients with different stages of prostate cancer, Oncol. Lett. 21 (5) (2021) 357.
[6] Y. Shiozawa, et al., Human prostate cancer metastases target the hematopoietic stem cell niche to establish footholds in mouse bone marrow, J. Clin. Invest. 121 (4) (2011) 1298–1312.
[7] Y. Shiozawa, et al., Annexin II/annexin II receptor axis regulates adhesion, migration, homing, and growth of prostate cancer, J. Cell. Biochem. 105 (2) (2008) 370–380.
[8] R.S. Taichman, et al., GAS6 receptor status is associated with dormancy and bone metastatic tumor formation, PLoS One 8 (4) (2013) e61873.
[9] M. Tanaka, S.S. Dykes, D.W. Siemann, Inhibition of the Axl pathway impairs breast and prostate cancer metastasis to the bones and bone remodeling, Clin. Exp. Metastasis 38 (3) (2021) 321–335.
[10] F.G.F. Tresguerres, et al., The osteocyte: a multifunctional cell within the bone, Ann. Anat. 227 (2020) 151422.
[11] M. Murshed, Mechanism of bone mineralization, Cold Spring Harb Perspect Med 8 (12) (2018).
[12] S.E. Noel, M.P. Santos, N.C. Wright, Racial and ethnic disparities in bone health and outcomes in the United States, J. Bone Miner. Res. 36 (10) (2021) 1881–1905.
[13] I.O.F. *Epidemiology of Osteoporosis and Fragility Fractures*. 2022 01/05/2023]; Available from: https://www.osteoporosis.foundation/facts-statistics/epidemiology-of-osteoporosis-and-fragility-fractures.
[14] V. Veldurthy, et al., Vitamin D, calcium homeostasis and aging, Bone Res 4 (2016) 16041.
[15] C. Cipriani, et al., The interplay between bone and glucose metabolism, Front. Endocrinol. 11 (2020) 122.
[16] K. Jackson, K.F. Moseley, Diabetes and bone fragility: SGLT2 inhibitor use in the context of renal and cardiovascular benefits, Curr. Osteoporos. Rep. 18 (5) (2020) 439–448.
[17] T. Teissier, et al., Crosstalk between senescent bone cells and the bone tissue microenvironment influences bone fragility during chronological age and in diabetes, Front. Physiol. 13 (2022) 812157.
[18] C. Ahn, J.H. Kang, E.B. Jeung, Calcium homeostasis in diabetes mellitus, J. Vet. Sci. 18 (3) (2017) 261–266.
[19] A.M.E. Badri, A. Salawu, J.E. Brown, Bone health in men with prostate cancer: review article, Curr. Osteoporos. Rep. 17 (6) (2019) 527–537.
[20] I. Tsaur, et al., Combining anticancer drugs with osteoprotective agents in prostate cancer-A contemporary update, Urol. Oncol. 36 (11) (2018) 488–497.
[21] M.C. Pinto, et al., Calcium signaling and cell proliferation, Cell. Signal. 27 (11) (2015) 2139–2149.
[22] A. Danese, et al., Cell death as a result of calcium signaling modulation: a cancer-centric prospective, Biochim. Biophys. Acta Mol. Cell Res. 1868 (8) (2021) 119061.
[23] S. Patergnani, et al., Various aspects of calcium signaling in the regulation of apoptosis, autophagy, cell proliferation, and cancer, Int. J. Mol. Sci. 21 (21) (2020).

[24] M.R. Smith, et al., Disease and host characteristics as predictors of time to first bone metastasis and death in men with progressive castration-resistant nonmetastatic prostate cancer, Cancer 117 (10) (2011) 2077–2085.
[25] C. Press, Plastic resin emerges as tiniest example of enduring COVID-19 supply chain crunch, in: CTV News, 2021.
[26] K. Sheridan, How Blackouts, Fires, and a Pandemic Are Driving Shortages of Pipette Tips — and Hobbling Science, Boston Globe Media Partners, 2021. STAT News.
[27] C. Kim, et al., Comparison of titanium soaked in 5 M NaOH or 5 M KOH solutions, Mater. Sci. Eng., C 33 (1) (2013) 327–339.
[28] C. Vaquette, et al., Effect of culture conditions and calcium phosphate coating on ectopic bone formation, Biomaterials 34 (22) (2013) 5538–5551.
[29] H. Kim, et al., Effect of remineralized collagen on dentin bond strength through calcium phosphate ion clusters or metastable calcium phosphate solution, Nanomaterials 10 (11) (2020).
[30] Y. Zhou, et al., Metascape provides a biologist-oriented resource for the analysis of systems-level datasets, Nat. Commun. 10 (1) (2019) 1523.
[31] L. Bubendorf, et al., Metastatic patterns of prostate cancer: an autopsy study of 1,589 patients, Hum. Pathol. 31 (5) (2000) 578–583.
[32] D. Schilling, et al., Isolated, disseminated and circulating tumour cells in prostate cancer, Nat. Rev. Urol. 9 (8) (2012) 448–463.
[33] Y. Shiozawa, et al., GAS6/AXL axis regulates prostate cancer invasion, proliferation, and survival in the bone marrow niche, Neoplasia 12 (2) (2010) 116–127.
[34] R. San Martin, et al., Tenascin-C and integrin alpha9 mediate interactions of prostate cancer with the bone microenvironment, Cancer Res. 77 (21) (2017) 5977–5988.
[35] H. Wang, et al., The osteogenic niche is a calcium reservoir of bone micrometastases and confers unexpected therapeutic vulnerability, Cancer Cell 34 (5) (2018) 823–839.e7.
[36] P.I. Croucher, M.M. McDonald, T.J. Martin, Bone metastasis: the importance of the neighbourhood, Nat. Rev. Cancer 16 (6) (2016) 373–386.
[37] J. Jeong, et al., Bioactive calcium phosphate materials and applications in bone regeneration, Biomater. Res. 23 (2019) 4.
[38] M. Brennan, et al., Biomimetic versus sintered macroporous calcium phosphate scaffolds enhanced bone regeneration and human mesenchymal stromal cell engraftment in calvarial defects, Acta Biomater. 135 (2021) 689–704.
[39] S.H. Maxian, J.P. Zawadsky, M.G. Dunn, Mechanical and histological evaluation of amorphous calcium phosphate and poorly crystallized hydroxyapatite coatings on titanium implants, J. Biomed. Mater. Res. 27 (6) (1993) 717–728.
[40] E.D. Eanes, I.H. Gillessen, A.S. Posner, Intermediate states in the precipitation of hydroxyapatite, Nature 208 (5008) (1965) 365–367.
[41] M. Edén, Structure and formation of amorphous calcium phosphate and its role as surface layer of nanocrystalline apatite: implications for bone mineralization, Materialia 17 (2021) 101107.
[42] A.L. Boskey, Amorphous calcium phosphate: the contention of bone, J. Dent. Res. 76 (8) (1997) 1433–1436.
[43] J. Mahamid, et al., Amorphous calcium phosphate is a major component of the forming fin bones of zebrafish: indications for an amorphous precursor phase, Proc. Natl. Acad. Sci. U.S.A. 105 (35) (2008) 12748–12753.
[44] A. Lotsari, et al., Transformation of amorphous calcium phosphate to bone-like apatite, Nat. Commun. 9 (1) (2018) 4170.
[45] A. Kaflak-Hachulska, A. Samoson, W. Kolodziejski, 1H MAS and 1H –> 31P CP/MAS NMR study of human bone mineral, Calcif. Tissue Int. 73 (5) (2003) 476–486.
[46] J.D. Termine, A.S. Posner, Amorphous/crystalline interrelationships in bone mineral, Calcif. Tissue Res. 1 (1) (1967) 8–23.
[47] S. El Badri, A. Salawu, J.E. Brown, Bone health in men with prostate cancer: review article, Curr. Osteoporos. Rep. 17 (6) (2019) 527–537.
[48] K. Hatano, N. Nonomura, Systemic Therapies for Metastatic Castration-Resistant Prostate Cancer: an Updated Review, 41, World J Mens Health, 2023.
[49] R. Kumar, et al., The testosterone paradox of advanced prostate cancer: mechanistic insights and clinical implications, Nat. Rev. Urol. (2022).
[50] N.V. Mohamad, I.N. Soelaiman, K.Y. Chin, A review on the effects of androgen deprivation therapy (ADT) on bone health status in men with prostate cancer, Endocr., Metab. Immune Disord.: Drug Targets 17 (4) (2017) 276–284.
[51] K. Fizazi, et al., Bone-related parameters are the main prognostic factors for overall survival in men with bone metastases from castration-resistant prostate cancer, Eur. Urol. 68 (1) (2015) 42–50.
[52] K.N. Chi, et al., A prognostic index model for predicting overall survival in patients with metastatic castration-resistant prostate cancer treated with abiraterone acetate after docetaxel, Ann. Oncol. 27 (3) (2016) 454–460.
[53] A. Bargiota, et al., Adverse effects of androgen deprivation therapy in patients with prostate cancer: focus on muscle and bone health, J buon 25 (3) (2020) 1286–1294.
[54] Z.W. Sharawi, et al., Calcium activation of the androgen receptor in prostate cells, Internet J. Endocrinol. 2023 (2023) 9907948.
[55] A. Heidenreich, et al., EAU guidelines on prostate cancer. Part II: treatment of advanced, relapsing, and castration-resistant prostate cancer, Eur. Urol. 65 (2) (2014) 467–479.
[56] G. Roviello, et al., Castration-resistant prostate cancer with bone metastases: toward the best therapeutic choice, Med. Oncol. 39 (10) (2022) 145.
[57] A. Davies, et al., Biological evolution of castration-resistant prostate cancer, Eur Urol Focus 5 (2) (2019) 147–154.
[58] D. Bello, et al., Androgen responsive adult human prostatic epithelial cell lines immortalized by human papillomavirus 18, Carcinogenesis 18 (6) (1997) 1215–1223.
[59] J.S. Horoszewicz, et al., The LNCaP cell line–a new model for studies on human prostatic carcinoma, Prog. Clin. Biol. Res. 37 (1980) 115–132.
[60] S. Korenchuk, et al., VCaP, a cell-based model system of human prostate cancer, In Vivo 15 (2) (2001) 163–168.
[61] N.M. Navone, et al., Establishment of two human prostate cancer cell lines derived from a single bone metastasis, Clin. Cancer Res. 3 (12 Pt 1) (1997) 2493–2500.